Sulfur-Tolerant Redox-Reversible Anode Material for Direct Hydrocarbon Solid Oxide Fuel Cells

Chenghao Yang, Zhibin Yang, Chao Jin, Guoliang Xiao, Fanglin Chen, and Minfang Han**

Solid oxide fuel cells (SOFCs) can convert chemical energy to electrical energy with high efficiency and fuel flexibility.[1–3] The conventional Ni-based anode has low tolerance to sulfur-contaminants in the fuel,[4] is vulnerable to deactivation by carbon build-up (coking) from direct oxidation of hydrocarbon fuels,[5] and suffers volume instability on redox cycling.[6,7] Many methods have been introduced to modify the Ni-based anode to achieve better sulfur tolerance and coking resistance. Replacing yttria-stabilized zirconia (YSZ) with doped ceria in the Ni-based cermets has shown some success, since Ce^{4+}/Ce^{3+} mixed-valent cation is catalytically active toward oxidation of CO and hydrocarbon fuels without causing carbon deposition.[8,9] Recently, $BaZr_{0.1}Ce_{0.7}Y_{0.2-x}Yb_xO_{3-\delta}$ (BZCYYb) has also been reported to greatly improve coking resistance and sulfur tolerance of the Ni-based anode.[10] However, cell performance drop was still observed after long-term test when these cells were subjected to H_2 contaminated with high concentration of H_2S.

Significant efforts have also been devoted to develop Ni-free anodes to alleviate carbon build-up, sulfur poisoning and volume instability problems encountered on Ni-based cermets anode. Among those, $(La_{0.75}Sr_{0.25})_{0.9}Cr_{0.5}Mn_{0.5}O_3$ (LSCM)[11] and $Sr_2MgMoO_{6-\delta}$ (SMM)[12] have been considered as successful candidates as SOFC anodes for direct utilization of hydrocarbon fuels. Although these approaches are promising, the catalytic activity of the reported ceramic anodes is still much lower than that of the conventional Ni-based anode. Alternatively, transition metals such as Cu or Fe, and alloys such as Ni-Cu, Ni-Co or Ni-Fe have been investigated to replace Ni for SOFC anode to improve the cell performance.[13–21] Although Cu-CeO_2-YSZ anode has showed good sulfur tolerance,[8,16] Cu is inactive for hydrocarbon oxidation and serves only as electronic conductor, resulting in limited cell power output. Further, Cu-based anode has potentially stability issues since Cu tends to coarsen at the typical SOFC operating temperatures. As for Fe, Ni-Co or Ni-Fe-based anodes, although they have shown excellent coking resistance, their sulfur tolerance has not been demonstrated.[18–21] Therefore, it is of great importance to develop an anode material that possesses a combined property of good sulfur tolerance, coking resistance and redox cyclability.

In this work, we report a novel composite anode consisting of K_2NiF_4-type structured $Pr_{0.8}Sr_{1.2}(Co,Fe)_{0.8}Nb_{0.2}O_{4+\delta}$ (K-PSCFN) matrix with homogeneously dispersed nano-sized Co-Fe alloy (CFA). This composite anode is obtained by annealing perovskite $Pr_{0.4}Sr_{0.6}Co_{0.2}Fe_{0.7}Nb_{0.1}O_{3-\delta}$ (P-PSCFN) in H_2 at 900 °C. K-PSCFN-CFA composite anode has demonstrated similar catalytic activity to Ni-based cermets anode, excellent sulfur tolerance and coking resistance. Moreover, K-PSCFN-CFA can be oxidized back to P-PSCFN in air at 900 °C, demonstrating excellent redox cyclability.

Figure 1A shows the typical performance of K-PSCFN-CFA|LSGM|P-PSCFN electrolyte-supported single cells using H_2, H_2 containing 50 or 100 ppm H_2S (H_2-50 ppm H_2S or H_2-100 ppm H_2S) as the fuel and ambient air as the oxidant. The cell maximum power density (P_{max}) in H_2 reached 0.96 W cm^{-2} at 850 °C. When the anode feeding gas was switched to H_2 containing 50 and 100 ppm H_2S, the P_{max} values were still 0.92 and 0.89 W cm^{-2} at 850 °C, respectively. However, when pure K-PSCFN was used as anode in a similar K-PSCFN|LSGM|P-PSCFN cell configuration, the P_{max} was only 0.21 W cm^{-2} in H_2 and 0.17 W cm^{-2} in H_2 containing 50 ppm H_2S at 850 °C (Figure S5), indicating that the CFA phase in the K-PSCFN-CFA composite has significant impact on the catalytic activity of the anode. The performance stability of the K-PSCFN|LSGM|P-PSCFN cells was tested under a constant current load of 0.3 A cm^{-2} in H_2 for 20 h and then under a constant current load of 0.2 A cm^{-2} in H_2-50 ppm H_2S at 850 °C (Figure S6). The cell exhibited relatively stable power output during 100 h operation, indicating that K-PSCFN anode has reasonable sulfur tolerance, but low catalytic activity toward H_2 oxidation. When the anode feeding gas was switched to CH_4, the cell performance dropped dramatically with P_{max} value of 0.086 W cm^{-2} at 850 °C (Figure 1B), indicating that pure K-PSCFN anode has relatively low catalytic activity towards methane oxidation. However, relatively high P_{max} of 0.6 W cm^{-2} in CH_4 and 0.94 W cm^{-2} in C_3H_8 were obtained at 850 °C for K-PSCFN-CFA|LSGM|P-PSCFN single cells using K-PSCFN-CFA composite anode (Figure 1B). Therefore, the enhanced performance of K-PSCFN-CFA anode in hydrogen/hydrocarbon can be mainly ascribed to the well dispersed nano-sized CFA phase in the K-PSCFN matrix, as indicated in the SEM images in **Figure 2**. The P-PSCFN was

Dr. C. Yang,[+] Z. Yang,[+] Dr. G. Xiao, Prof. F. Chen
Department of Mechanical Engineering
University of South Carolina
Columbia, SC 29208, USA
E-mail: chenfa@cec.sc.edu
Dr. C. Jin[+]
School of Energy
Soochow University
Suzhou 215006, P.R. China
Z. Yang, Prof. M. Han
Union Research Center of Fuel Cell
School of Chemical & Environmental Engineering
China University of Mining & Technology
Beijing, 100083, P.R. China
E-mail: hanminfang@sina.com
[+] These authors contributed equally to this work.

DOI: 10.1002/adma.201104852

ADVANCED MATERIALS
www.advmat.de

www.MaterialsViews.com

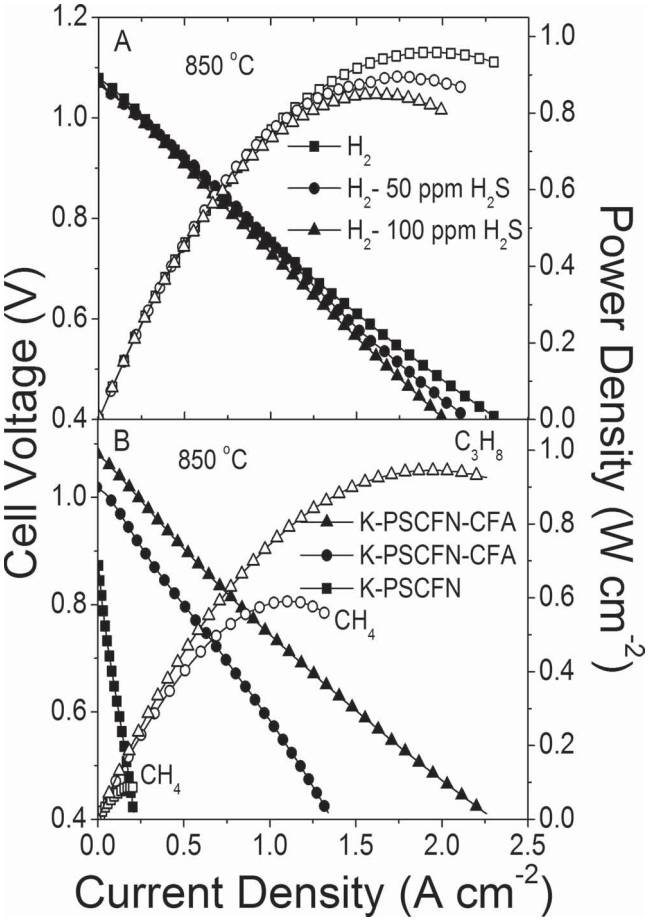

Figure 1. Cell voltage and power density as a function of current density for the LSGM electrolyte-supported single cells with P-PSCFN as cathode and (**A**) K-PSCFN-CFA as anode in H_2 and H_2/H_2S at 850 °C; and (**B**) with K-PSCFN-CFA or K-PSCFN as anode in CH_4 and C_3H_8 at 850 °C, respectively.

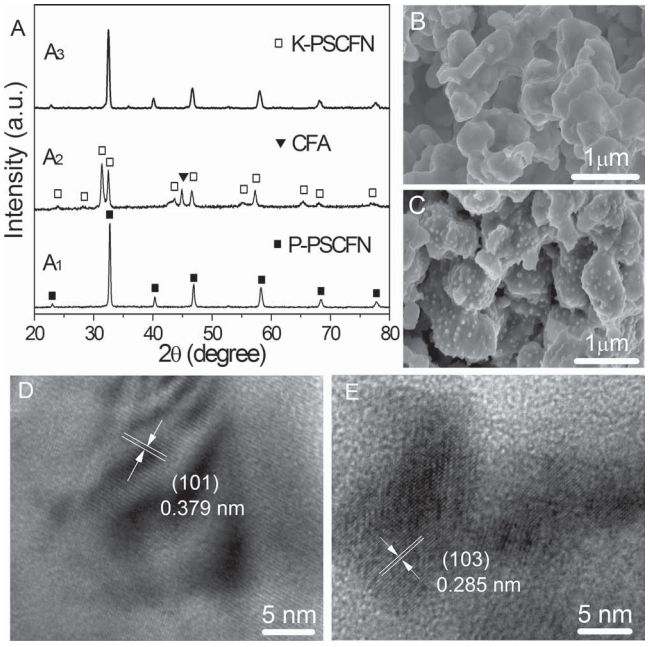

Figure 2. (A) X-ray diffraction (XRD) patterns of (A1) P-PSCFN sintered at 1050 °C in air; (A2) P-PSCFN annealed in 5 vol% H_2–95 vol% N_2 at 900 °C; and (A3) K-PSCFN-CFA composite re-oxidized in air at 900 °C; (B and C) SEM images and (D and E) HRTEM images of P-PSCFN before and after being reduced in H_2 at 900 °C.

transformed to a composite of K-PSCFN matrix with uniformly dispersed nano-sized CFA particles (~50 nm) after calcining P-PSCFN in H_2 at 900 °C (Figure 2C and Figure S2A). Further, it has been demonstrated that the K-PSCFN-CFA composite can be re-oxidized back to P-PSCFN at 900 °C in air (Figure 2A). High-resolution transmission electron microscopy (HRTEM) analysis of P-PSCFN has revealed a lattice spacing of 0.379 nm (Figure 2D), consistent with the 0.374 nm separation between two (101) planes of the P-PSCFN crystalline structure (space group Pnma) determined by the XRD analysis. However, a lattice spacing of 0.285 nm has been obtained after P-PSCFN has been reduced in H_2 at 900 °C (Figure 2E), similar to the lattice spacing of 0.284 nm between two (103) planes in the K-PSCFN crystalline structure (space group I41) determined by the XRD analysis.

The anode polarization resistance was evaluated using a symmetric half cell configuration with K-PSCFN-CFA as both working and counter electrodes on a LSGM electrolyte in H_2, and the results at different temperatures are shown in **Figure 3**. The anode polarization resistances are 0.44 Ω cm^2 at 800 °C, 0.31Ω cm^2 at 850 °C and 0.16 Ω cm^2 at 900°C, which are much smaller than that of the LSCM ceramic anode[11] and comparable to that of the traditional Ni-YSZ[22] or Ni-GDC anode.[23]

The electrochemical performance of the K-PSCFN-CFA anode has also been studied in LSGM electrolyte-supported single cells with $Ba_{0.9}Co_{0.7}Fe_{0.2}Nb_{0.1}O_{3-\delta}$ (BCFN) as the cathode. BCFN has recently been reported to be a promising SOFC cathode material, possessing good chemical stability but similar catalytic activity for

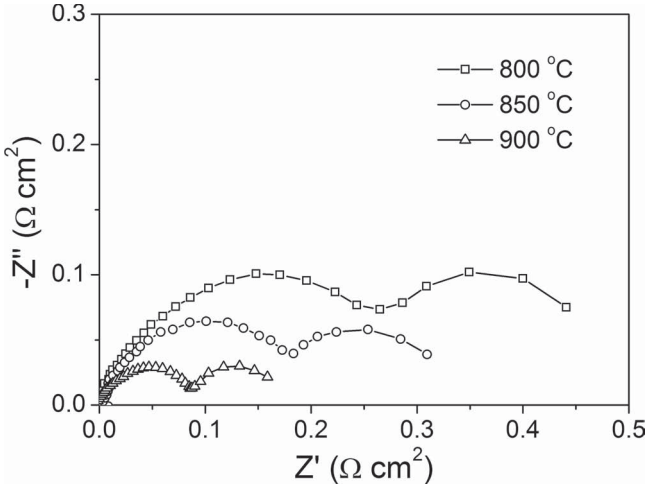

Figure 3. Impedance spectra of the symmetric half cell with K-PSCFN-CFA composite electrode measured in H_2 at 800, 850, and 900 °C, respectively. The ohmic contribution from the LSGM electrolyte has been subtracted from the overall impedance spectra.

Adv. Mater. **2012**,
DOI: 10.1002/adma.201104852

oxygen reduction to $Ba_{0.5}Sr_{0.5}Co_{0.8}Fe_{0.2}O_{3-\delta}$ (BSCF).[24] P_{max} of the cell were 0.36, 0.62, 0.9, 1.13, and 1.45 W cm^{-2} at 700, 750, 800, 850 and 900 °C, respectively (Figure S7), comparable to those of the cells with Ni-based anode at similar testing conditions, e.g., at 800 °C, 0.618 W cm^{-2} of Ni-GDC|GDC|BCFN single cells,[25] 0.98 W cm^{-2} of Ni-GDC|LSGM|BCFN single cells,[26] and 0.92 W cm^{-2} of Ni-SDC|LSGM|LSCF (SDC, $Sm_{0.2}Ce_{0.8}O_{1.9}$; LSCF, $La_{0.6}Sr_{0.4}Co_{0.8}Fe_{0.2}O_{3-\delta}$) single cells (Table S1).[27] On the other hand, they are superior to those of cells using other Ni-free sulfur tolerant ceramic anodes, e.g., $La_{0.7}Sr_{0.3}VO_3$ (LSV),[28] $La_{0.2}Sr_{0.8}TiO_3$ (LST),[29,30] $Sr_{0.88}Y_{0.08}TiO_{3-\delta}$ (SYT),[31] $La_{0.75}Sr_{0.25}Cr_{0.5}Mn_{0.5}O_{3-\delta}$ (LSCM),[32] $Sr_2MgMoO_{6-\delta}$ (SMM)[12] and $Sr_2Fe_{1.5}Mn_{0.5}O_{6-\delta}$ (SFM) (Table S1).[7] Moreover, it should be noted that all the button cells in this study were fabricated by screen-printing the electrode ink directly onto either surface of the 300-μm thick LSGM electrolyte. Therefore, using a thinner electrolyte would greatly reduce the cell ohmic resistance while optimizing electrode microstructure through adding pore formers to the electrode ink or infiltration of fine electrode particles would dramatically reduce the cell electrode polarization resistance, consequently further increasing the cell performance and lowering the cell operating temperature.

In order to evaluate the chemical compatibility of K-PSCFN-CFA anode material with YSZ electrolyte material, the P-PSCFN-YSZ mixture has been sintered in air at 900 °C for 10 h while the K-PSCFN-CFA-YSZ mixture has been sintered in H_2 at 900 °C for 10 h. In comparison to the XRD patterns of pure YSZ, P-PSCFN and K-PSCFN-CFA powders, XRD pattern of the mixture of P-PSCFN and YSZ as well as that of the mixture of K-PSCFN-CFA and YSZ sintered at 900 °C showed no observable impurity phases (Figures S12 and S13). In addition, single cells with the cell configuration of K-PSCFN-CFA|YSZ|BCFN have also been evaluated using hydrogen as fuel and ambient air as oxidant, showing relatively stable cell performance under constant current density of 0.3 A cm^{-2} at 800 °C (Figure S15), indicating that the K-PSCFN-CFA is chemically compatible with YSZ electrolyte at the cell fabrication and testing conditions studied in this work.

To determine the sulfur tolerance of the K-PSCFN-CFA anode, the voltage of K-PSCFN-CFA|LSGM|P-PSCFN single cells was recorded as a function of time under a constant current load of 0.6 A cm^{-2} operating in H_2 containing 50 ppm H_2S at 800 °C, as shown in **Figure 4**A. The cell showed excellent stability using H_2-50 ppm H_2S as the fuel at 800 °C and no significant power output degradation was observed for ~500 h operation. When the cell testing temperature was lowered to 700 and 750 °C, the cell power output was still very stable under a constant current load of 0.2 A cm^{-2} at 700 °C and 0.4 A cm^{-2} at 750 °C in H_2-50 ppm H_2S (Figure S16), indicating that the K-PSCFN-CFA anode possesses excellent tolerance to sulfur poisoning. In contrast, the performance of LSGM electrolyte-supported cells with Ni-GDC anode and BCFN cathode degraded rapidly in H_2-50 ppm H_2S at 800 °C (Figure S17).

The coking resistance for direct oxidation of hydrocarbon fuels of the K-PSCFN-CFA|LSGM|P-PSCFN cells is exhibited in Figure 4B. When CH_4 or C_3H_8 was supplied to the anode, no significant cell voltage change was observed under a constant current load of 0.2 A cm^{-2} using CH_4 or 0.4 A cm^{-2} using C_3H_8 as the fuel at 800 °C, respectively. It is well known that carbon can easily build up on conventional Ni-based anode when directly operating on dry CH_4.[9,33,34] According to the density functional theory (DFT) calculations and experimental studies reported previously, bi-metallic alloy can preferentially oxidize carbon atoms and fragments, removing them from the surface of the electrocatalyst rather than forming carbon-carbon bonds as does in monometallic Ni.[20,21] These results suggest that K-PSCFN-CFA composite is a promising anode material with sulfur tolerance and coking resistance.

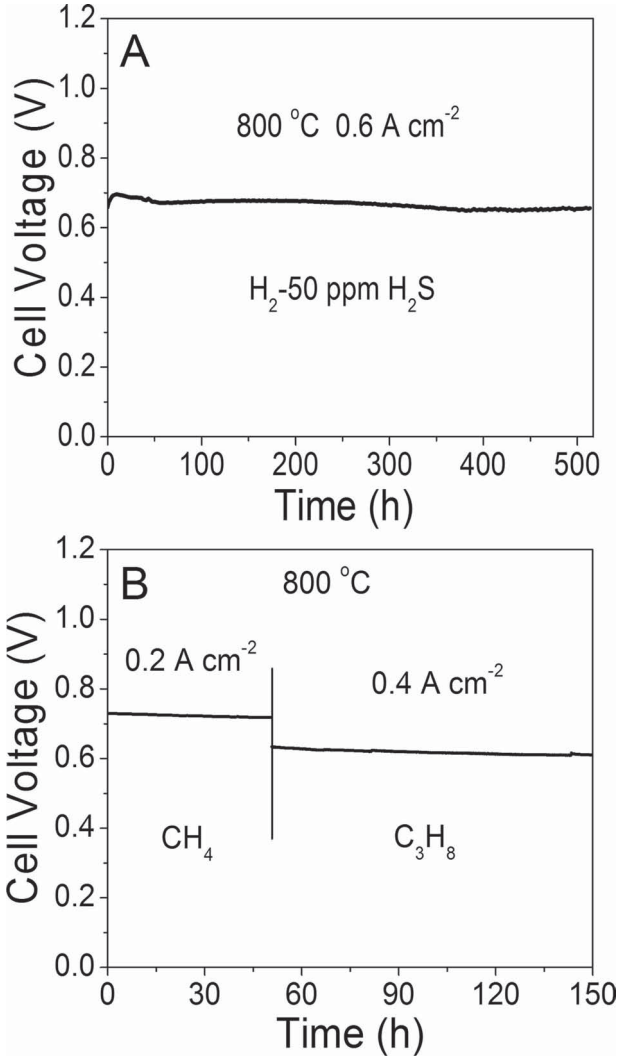

Figure 4. Cell voltage as a function of time at 800 °C for the K-PSCFN-CFA|LSGM|P-PSCFN single cells operated under a constant current load of (A) 0.6 A cm^{-2} in H_2-50 ppm H_2S, and (B) 0.2 A cm^{-2} in CH_4 and 0.4 A cm^{-2} in C_3H_8.

Finally, the cyclic stability of the K-PSCFN-CFA composite anode was demonstrated in single cells with the configuration of K-PSCFN-CFA|LSGM|P-PSCFN. The cell was initially operated under a constant current load of 0.6 A cm^{-2} in H_2 at 850 °C for 24 h to obtain a stable cell performance. The current load was then removed and a voltage-current (V-I) curve was measured to obtain the maximum power density. Subsequently,

DOI: 10.1002/adma.201104852

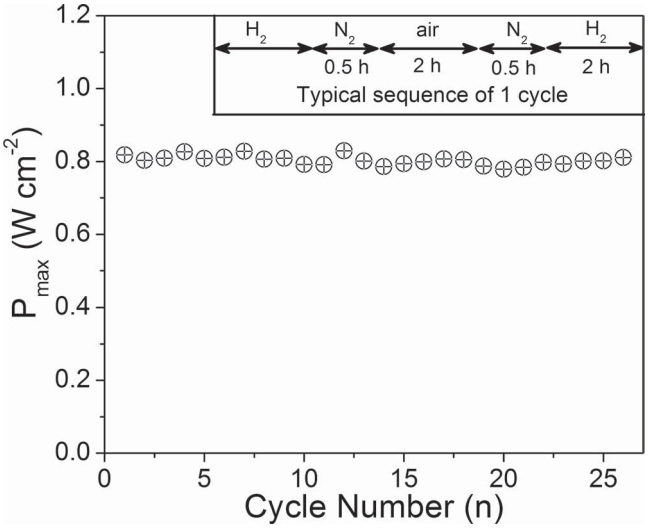

Figure 5. Redox cycling stability of the K-PSCFN-CFA composite anode in single cells with cell configuration of K-PSCFN-CFA|LSGM|P-PSCFN at 850 °C. In each cycle, after the V-I curve was measured, H_2 flow to the anode was stopped while the cell was still maintained at 850 °C and N_2 was used to purge the anode for 0.5 h. Air was subsequently supplied to the anode while the furnace was heated up to 900 °C and held for 2 h. After the air flow was terminated, N_2 was used to purge the anode for 0.5 h. Finally, H_2 was supplied to the anode for 2 h while the cell was cooled down to 850 °C.

the K-PSCFN-CFA anode was subjected to the cyclic test by switching the anode gas stream between H_2 and air, and the cell maximum power density were recorded after each cyclic test. As presented in **Figure 5**, the cell maximum power output was not affected by the redox cycling of the anode during a total of 26 cyclic testing, indicating that the K-PSCFN-CFA has excellent redox-reversibility.

In summary, a novel composite anode consisting of K-PSCFN matrix with uniformly dispersed nano-sized Co-Fe alloy has shown comparable catalytic activity for fuel oxidation to the Ni-based cermets anode. This novel composite anode demonstrates good electrical conductivity and excellent coking resistance and sulfur tolerance. Moreover, LSGM electrolyte-supported single cells with K-PSCFN-CFA as the anode and P-PSCFN as the cathode exhibits high power output and excellent stability in redox cycling test.

Experimental Section

P-PSCFN and K-PSCFN powders were synthesized using a solid-state reaction method. The precursor powders with stoichiometric amount of $Pr(NO_3)_3{\cdot}6H_2O$, $SrCO_3$, $Co(NO_3)_2{\cdot}6H_2O$, Fe_2O_3 and Nb_2O_5 were mixed by ball milling. Calcination of the precursor powders was performed at 1050 °C for 5 h in air to obtain pure phase. The $La_{0.8}Sr_{0.2}Ga_{0.83}Mg_{0.17}O_{3-\delta}$ (LSGM) and $Ba_{0.9}Co_{0.7}Fe_{0.2}Nb_{0.1}O_{3-\delta}$ (BCFN) powders were fabricated by a solid-state reaction method, and the GDC powders were prepared by a sol-gel process as described previously.[24] Single cells of K-PSCFN-CFA|LSGM|BCFN, K-PSCFN-CFA|LSGM|PSCFN, and K-PSCFN|LSGM|BCFN studied in this work were LSGM electrolyte-supported cells. LSGM electrolyte substrates were formed by dry-pressing LSGM powders uniaxially under 200 MPa, and followed by sintering at 1450 °C in air for 10 h. The thickness of the LSGM electrolyte was about 300 μm. The electrode ink consisting of P-PSCFN or BCFN powders and Heraeus binder V-006 (weight ratio of 1:1) was applied to the surface of the sintered LSGM pellet by screen-printing method, and then fired at 1000 °C in air for 2 h. The porous electrode had a thickness of about 30 μm and an effective area of 0.33 cm^2. To avoid potential catalytic influence on fuel oxidation, Au slurry was printed on the surface of the anode as current collector. Pt slurry was printed on the surface of the cathode as current collector. For the chemical compatibility study of the K-PSCFN-CFA anode with YSZ electrolyte (~300 μm thickness), the processing and testing temperatures are not higher than 900 °C. Since most Co-containing electrode materials have been reported to be chemically incompatible with the YSZ electrolyte at high temperatures,[35,36] a thin ceria-based buffer layer should be employed to prevent the potential reaction between the K-PSCFN-CFA electrode and YSZ electrolyte if a higher processing temperature is needed.[37]

Electrical conductivity of sintered K-PSCFN-CFA or P-PSCFN bar samples was measured using DC four-probe measurement. Four platinum wires were attached to the bar with platinum paste. The electrical conductivity of K-PSCFN-CFA was studied in 5 vol.% H_2-95 vol.% N_2, while that of P-PSCFN was measured in Air and N_2 at different temperatures.

Button cells were sealed to one end of an alumina tube with a ceramic paste (Aremco-552). The cells were heated up to 800 °C in air. At 800 °C, prior to the flow of H_2 to the anode, N_2 was used to purge the anode side. The cell was heated to 900 °C and held for 1 h to ensure that the P-PSCFN anode was fully annealed. After that, the fuel cells were cooled to 750–850 °C and the electrochemical testing was performed. The electrochemical impedance spectra were typically measured in the frequency range from 0.01 Hz to 1 MHz with IM6 Electrochemical Workstations. All fuel cells were first conditioned at a constant current density in pure H_2 to obtain steady state performance before switching to H_2 containing H_2S or hydrocarbon fuel. Since H_2S can dissolve in water, H_2 containing 50 or 100 ppm H_2S were introduced directly to the cell, and a separate flow of H_2 was passed through a water bubbler at room temperature to bring water vapor into the anode. The fuel flow rate was 40 mL min^{-1}, and ambient air was used as the oxidant.

The X-ray diffraction (XRD) pattern was recorded on an Rigaku D/Max 2100 Powder X-ray Diffractometer with a Cu-Kα radiation (λ = 1.5418 Å), employing a scan rate of 5 deg min^{-1} in the 2θ range from 20° to 80°. The microstructure of the powders and the electrodes were characterized using a scanning electron microscopy (SEM, FEI Quanta 200), a scanning transmission electron microscopy (STEM, Hitachi, HD2000 ultrathin film evaluation system) equipped with an energy dispersive spectroscopy (EDS) analyzer, and a high-resolution transmission electron microscopy (HRTEM).

Supporting Information

Supporting Information is available from the Wiley Online Library or from the author.

Acknowledgements

Financial support from the HeteroFoaM Center (Heterogeneous Functional Materials for Energy Systems), an EFRC funded by DoE-BES (award no DE-SC0001061) and NSF of China (50730004) is greatly appreciated.

Received: December 20, 2011
Published online:

DOI: 10.1002/adma.201104852

[1] R. M. Ormerod, *Chem. Soc. Rev.* **2003**, *32*, 17.
[2] A. J. Jacobson, *Chem. Mater.* **2010**, *22*, 660.
[3] A. Orera, P. R. Slater, *Chem. Mater.* **2010**, *22*, 675.
[4] M. Y. Gong, X. B. Liu, J. Trembly, C. Johnson, *J. Power Sources* **2007**, *168*, 289.
[5] Z. L. Zhan, S. A. Barnett, *Science* **2005**, *308*, 844.
[6] D. M. Bastidas, S. W. Tao, J. T. S. Irvine, *J. Mater. Chem.* **2006**, *16*, 1603.
[7] Q. Liu, X. H. Dong, G. L. Xiao, F. Zhao, F. L. Chen, *Adv. Mater.* **2010**, *22*, 5478.
[8] J. B. Goodenough, Y. H. Huang, *J. Power Sources* **2007**, *173*, 1.
[9] J. P. Trembly, A. I. Marquez, T. R. Ohrn, D. J. Bayless, *J. Power Sources* **2006**, *158*, 263.
[10] L. Yang, S. Z. Wang, K. Blinn, M. F. Liu, Z. Liu, Z. Cheng, M. L. Liu, *Science* **2009**, *326*, 126.
[11] S. W. Tao, J. T. S. Irvine, *Nat. Mater.* **2003**, *2*, 320.
[12] Y. H. Huang, R. I. Dass, Z. L. Xing, J. B. Goodenough, *Science* **2006**, *312*, 254.
[13] E. P. Murray, T. Tsai, S. A. Barnett, *Nature* **1999**, *400*, 649.
[14] S. Park, J. M. Vohs, R. J. Gorte, *Nature* **2000**, *404*, 265.
[15] H. Devianto, S. P. Yoon, S. W. Nam, J. Han, T. Lim, *J. Power Sources* **2006**, *159*, 1147.
[16] H. P. He, R. J. Gorte, J. M. Vohs, *Eletrochem. Solid-State Lett.* **2005**, *8*, A279.
[17] H. Kim, C. Lu, W. L. Worrell, J. M. Vohs, R. J. Gorte, *J. Electrochem. Soc.* **2002**, *149*, A247.
[18] T. Horita, N. Sakai, T. Kawada, M. Yokokawa, M. Dokiya, *J. Electrochem. Soc.* **1996**, *143*, 1161.
[19] B. Huang, S. R. Wang, R. Z. Liu, T. L.Wen, *J. Power Sources* **2007**, *167*, 288.
[20] E. Nikolla, J. Schwank, S. Linic, *J. Electrochem. Soc.* **2009**, *156*, B1312.
[21] W. An, D. Gatewood, B. Dunlap, C. H. Turner, *J. Power Sources* **2011**, *196*, 4724.
[22] T. Suzuki, M. Awano, P. Jasinski, V. Petrovsky, H. U. Anderson, *Solid State Ionics* **2006**, *177*, 2071.
[23] S. P. Jiang, S. Zhang, Y. D. Zhen, A. P. Koh, *Electrochem. Solid-State Lett.* **2004**, *7*, A282.
[24] Z. B. Yang, C. H. Yang, C. Jin, M. F. Han, F. Chen, *Electrochem. Commun.* **2011**, *13*, 882.
[25] S. Q. Lü, Y. Ji, X. W. Meng, G. H. Long, T. Wei, Y. L. Zhang, T. Q. Lü, *Electrochem. Solid-State Lett.* **2009**, *12*, B103.
[26] Z. B. Yang, C. H. Yang, B. Xiong, M. F. Han, F. Chen, *J. Power Sources* **2011**, *196*, 9164.
[27] W. M. Guo, J. Liu, C. Jin, H. B. Gao, Y. H. Zhang, *J. Alloys Compd.* **2009**, *473*, 43.
[28] L. Aguilar, S. W. Zha, S. W. Li, J. Winnick, M. L. Liu, *Electrochem. Solid-State Lett.* **2004**, *7*, A324.
[29] K. B. Yoo, G. M. Choi, *Solid State Ionics* **2009**, *180*, 867.
[30] K. B. Yoo, G. M. Choi, *Solid State Ionics* **2011**, *192*, 515.
[31] X. C. Lu, J. H. Zhu, Z. G. Yang, G. G. Xia, J. W. Stevenson, *J Power Sources* **2009**, *192*, 381.
[32] J. Peña-Martínez, D. Marrero-López, J. C. Ruiz-Morales, B. E. Buergler, P. Núñez, L. J. Gauckler, *Solid State Ionics* **2006**, *177*, 2143.
[33] H. Kan, H. Lee, *Catal. Commun.* **2010**, *12*, 36.
[34] J. Wang, J. Jiang, T. Huang, *J. Power Sources* **2003**, *122*, 122.
[35] O. Yamamoto, Y. Takeda, R. Kanno, M. Noda, *Solid State Ionics* **1987**, *22*, 241.
[36] H. Y. Tu, Y. Takeda, N. Imanishi, O. Yamamoto, *Solid State Ionics* **1999**, *117*, 277.
[37] J. W. Yun, S. P. Yoon, S. Park, J. Han, S. W. Nam, T. H. Lim, J. S. Kim, *Int. J. Hydrogen Energy* **2009**, *34*, 9213.

ADVANCED MATERIALS

Supporting Information

for *Adv. Mater.*, DOI: 10.1002/adma. **201104852**

Sulfur-Tolerant Redox-Reversible Anode Material for Direct Hydrocarbon Solid Oxide Fuel Cells

*Chenghao Yang , Zhibin Yang , Chao Jin , Guoliang Xiao , Fanglin Chen , * and Minfang Han **

Submitted to ADVANCED MATERIALS

Supporting Information: Sulfur-Tolerant Redox-Reversible Anode Material for Direct Hydrocarbon Solid Oxide Fuel Cells

By *Chenghao Yang, Zhibin Yang, Chao Jin, Guoliang Xiao, Fanglin Chen,* and Minfang Han**

Dr. C. Yang,[+] Z. Yang,[+] Dr. G. Xiao, Prof. F. Chen
Department of Mechanical Engineering
University of South Carolina
Columbia, SC 29208, USA
E-mail: chenfa@cec.sc.edu (F. Chen)

Dr. C. Jin[+]
School of Energy
Soochow University
Suzhou 215006, P.R. China

Z. Yang,[+] Prof. M. Han
Union Research Center of Fuel Cell
School of Chemical & Environmental Engineering
China University of Mining & Technology
Beijing, 100083, P.R. China
Email: hanminfang@sina.com (M. Han)

[+] These authors contributed equally to this work.

Table S1. Maximum power densities (P_{max}) of the LSGM electrolyte supported cell with K-PSCFN-CFA anode compared with the cells with Ni-based or ceramic anodes and similar configuration in H_2 at elevated temperature.

Anode material	Cell configuration	Testing temperature (^oC)	Maximum power density (P_{max}, W cm^{-2})	Reference
K-PSCFN-CFA	K-PSCFN-CFA|LSGM|BCFN	800	0.9	
Ni-GDC	Ni-GDC|GDC|BCFN	800	0.618	[25]
	Ni-GDC|LDC|LSGM|BCFN	800	0.98	[26]
	Ni-SDC|LDC|LSGM|LSCF	800	0.92	[27]
LSV	LSV|YSZ|SSC-GDC	800	0.14	[28]
LST	LST|LSGM|BSCF	800	0.06	[29,30]
SYT	Pd-SYT-LDC|LDC|LSGM|SSC	800	0.577	[31]
LSCM	LSCM|LSGM|BSCF	800	0.166	[32]
SMM	SMM|LDC|LSGM|SCF	800	0.838	[12]
SFM	SFM|LSGM|SFM	800	0.5	[7]

SSC: $Sm_{0.5}Sr_{0.5}CoO_3$. LDC: $La_{0.4}Ce_{0.6}O_{1.8}$. SCF: $SrCo_{0.8}Fe_{0.2}O_{3-\delta}$.

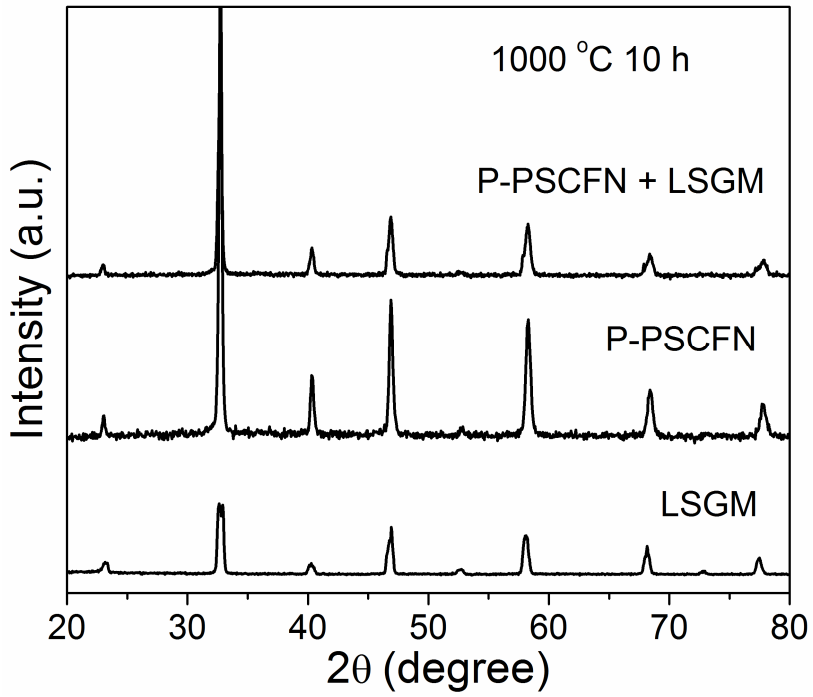

Figure S1. X-ray diffraction patterns (XRD) of perovskite $Pr_{0.4}Sr_{0.6}Co_{0.2}Fe_{0.7}Nb_{0.1}O_{3-\delta}$ (P-PSCFN) powders, pure $La_{0.8}Sr_{0.2}Ga_{0.83}Mg_{0.17}O_{3-\delta}$ (LSGM) powders, and X-ray diffraction pattern of P-PSCFN+LSGM mixture sintered in air at 1000 ^{o}C for 10 h.

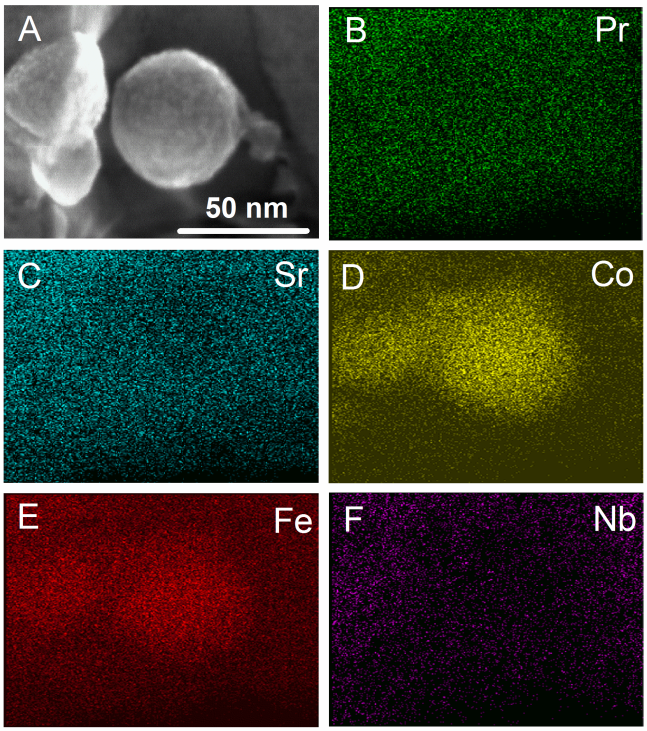

Figure S2. Pr, Sr, Co, Fe and Nb mapping analysis of the K_2NiF_4-type structured $Pr_{0.8}Sr_{1.2}(Co,Fe)_{0.8}Nb_{0.2}O_{4+\delta}$ (K-PSCFN) matrix with homogenously dispersed nano-sized Co-Fe alloy (CFA) composite anode surface after P-PSCFN being reduced by H_2 at 900 ^oC for 10h.

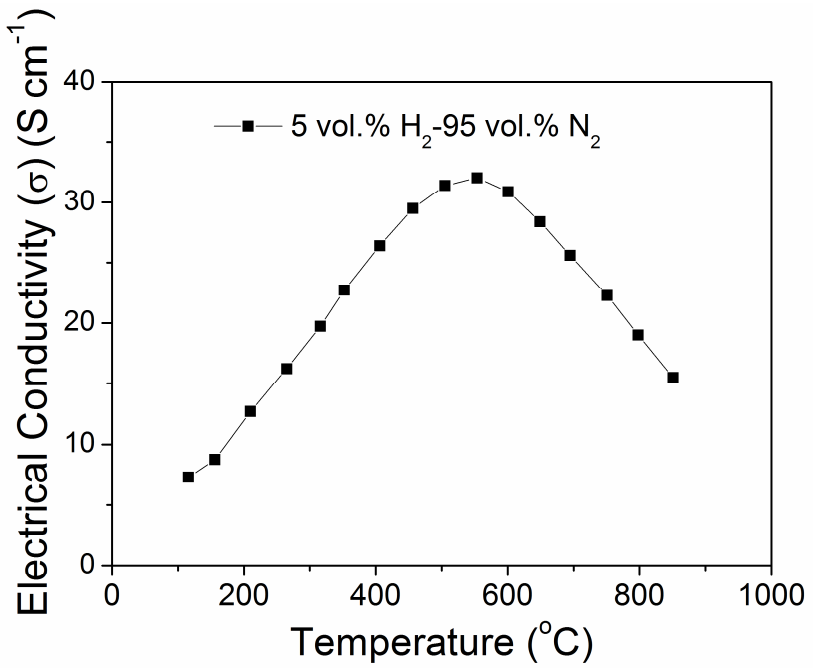

Figure S3. The electrical conductivity of K-PSCFN-CFA in 5 vol% H_2-95 vol% N_2.

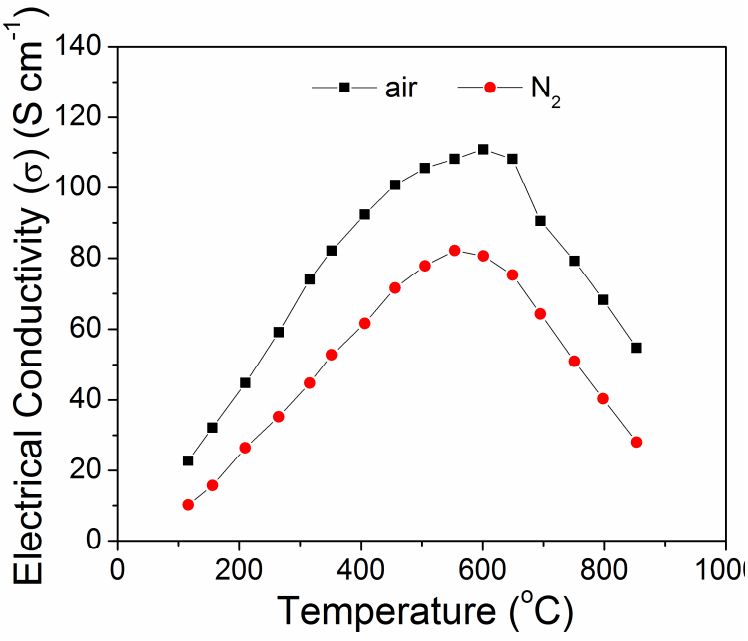

Figure S4. The electrical conductivity of P-PSCFN in air and N_2.

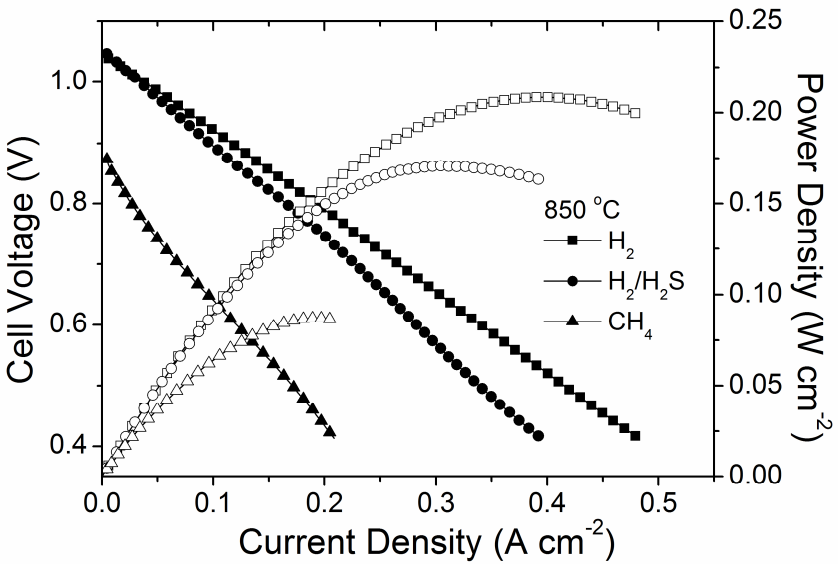

Figure S5. Current density-voltage and power density curves for K-PSCFN|LSGM|P-PSCFN cells with K-PSCFN as the anode operated at 850 ^{o}C, with H_2, H_2 containing 50 ppm H_2S and CH_4 as the fuel and ambient air as the oxidant, respectively.

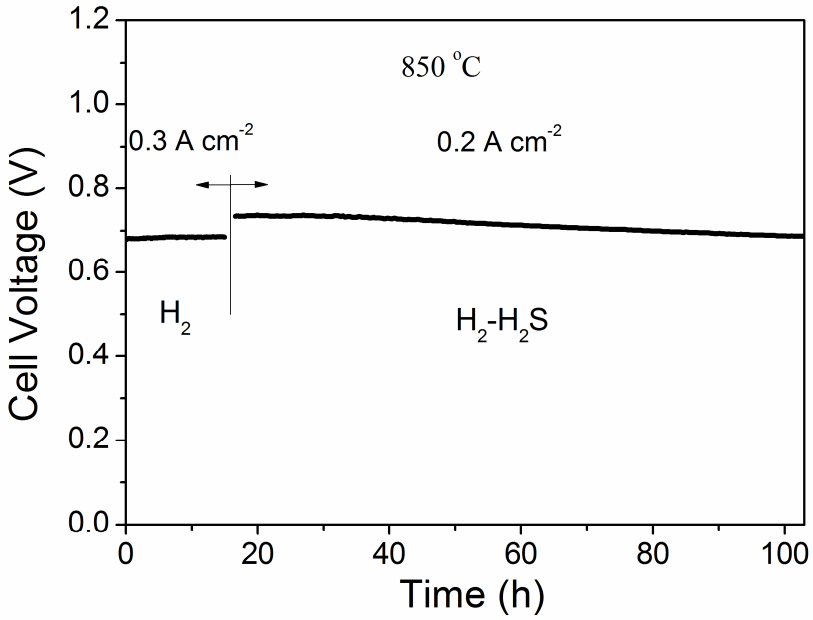

Figure S6. Cell voltage of K-PSCFN|LSGM|P-PSCFN cells with K-PSCFN as the anode operated under a constant current load of 0.3 A cm^{-2} in H_2, and 0.2 A cm^{-2} with H_2 containing 50 ppm H_2S as the fuel and air as the oxidant at 850 ^oC, respectively.

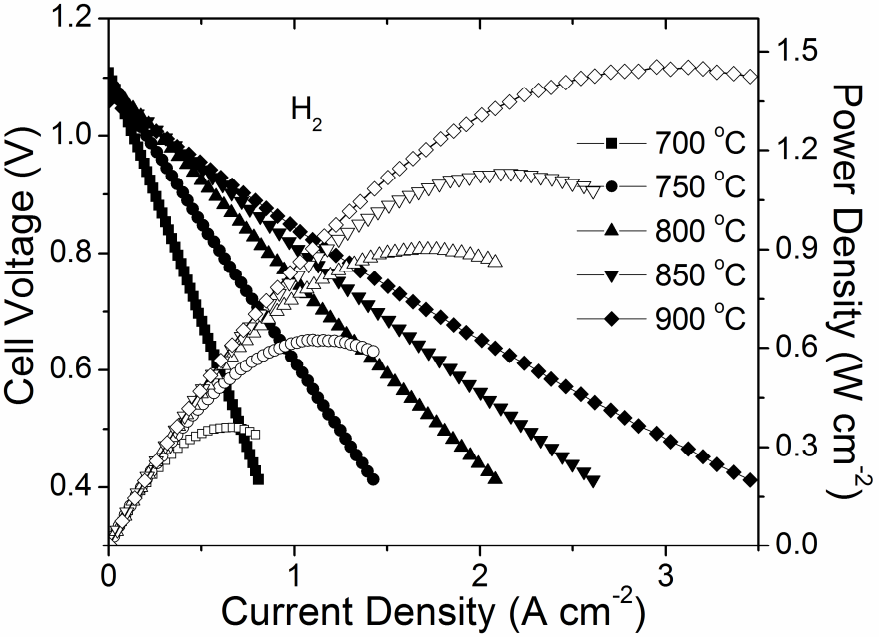

Figure S7. Current density-voltage and power density curves for K-PSCFN-CFA|LSGM|BCFN cell operating from 700 to 900 ^{o}C with H_2 as fuel and ambient air as oxidant. BCFN represents $Ba_{0.9}Co_{0.7}Fe_{0.2}Nb_{0.1}O_{3-\delta}$.

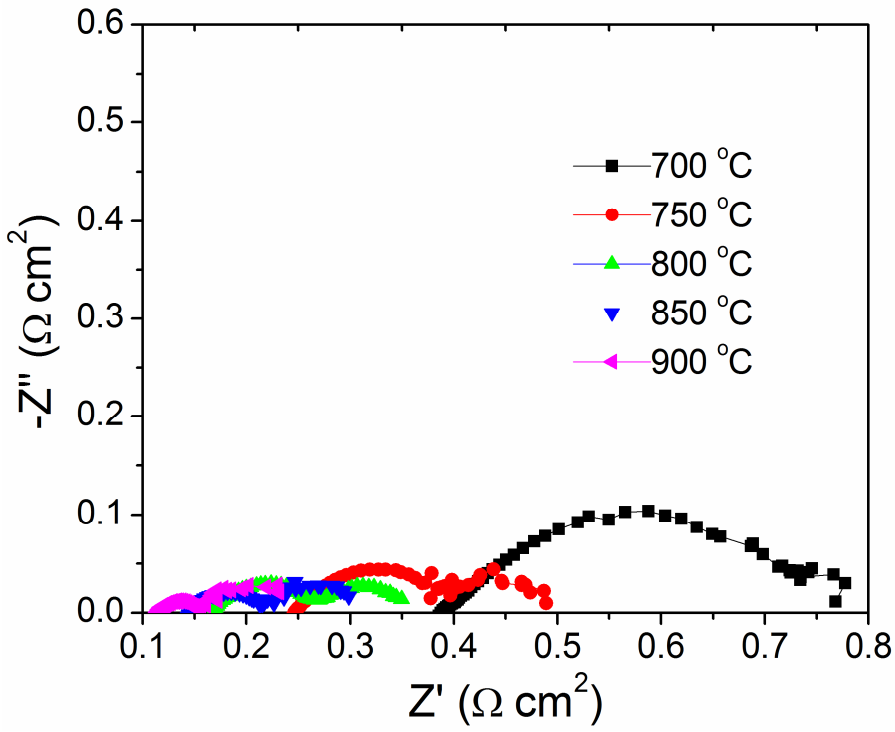

Figure S8. Impedance sprectra of K-PSCFN-CFA|LSGM|BCFN cell measured from 650 ^{o}C to 900 ^{o}C with H_2 as fuel and ambient air as the oxidant.

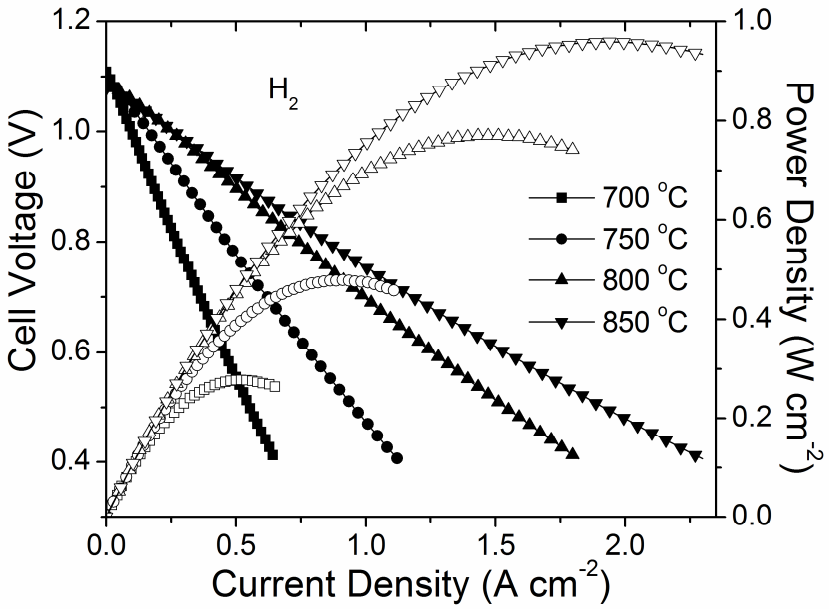

Figure S9. Current density-voltage and power density curves for single cells with the configuration of K-PSCFN-CFA|LSGM|P-PSCFN operating from 700 to 850 ^{o}C with H_2 as the fuel and ambient air as the oxidant.

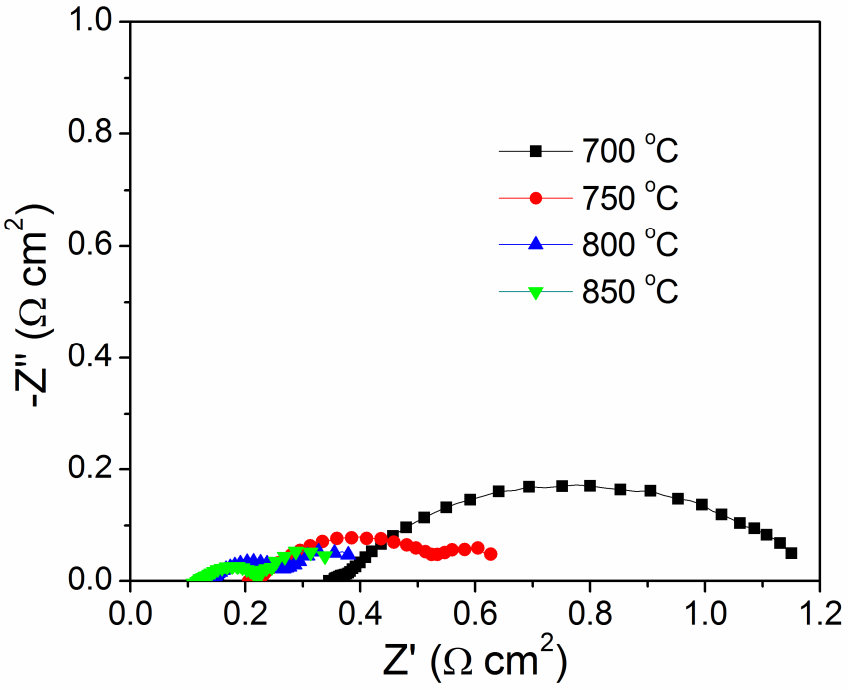

Figure S10. Impedance sprectra of K-PSCFN-CFA|LSGM|P-PSCFN cell measured from 700 to 850 ^{o}C with H_2 as the fuel and air as the oxidant.

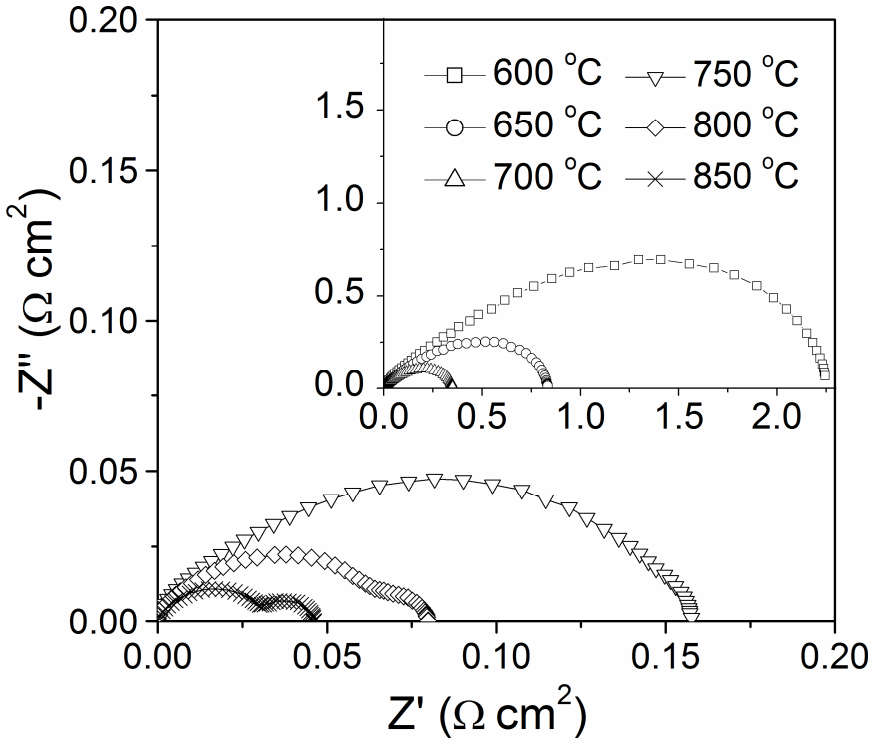

Figure S11. Impedance spectra of symmetric half cells using P-PSCFN as the electrode and LSGM as the electrolyte tested in air from 600 to 850 ^{o}C.

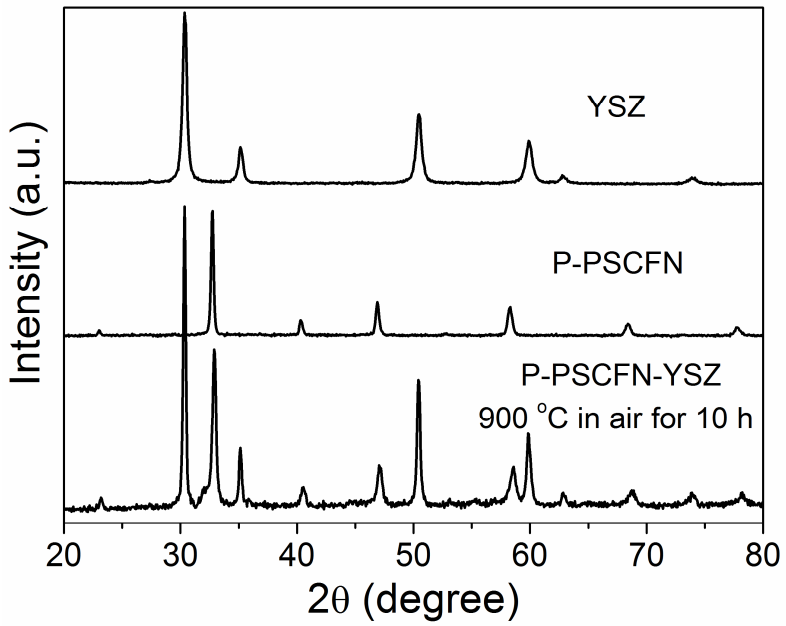

Figure S12. X-ray diffraction (XRD) patterns of (**A**) YSZ, (**B**) P-PSCFN and (**C**) P-PSCFN-YSZ sintered in air at 900 ^{o}C for 10 h.

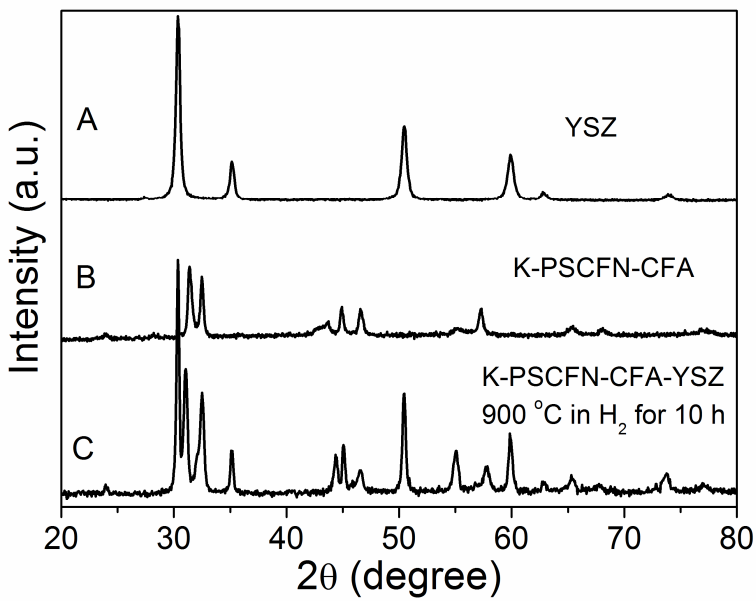

Figure S13. X-ray diffraction (XRD) patterns of (**A**) YSZ, (**B**) K-PSCFN-CFA and (**C**) K-PSCFN-CFA-YSZ sintered in H_2 at 900 ^oC for 10 h.

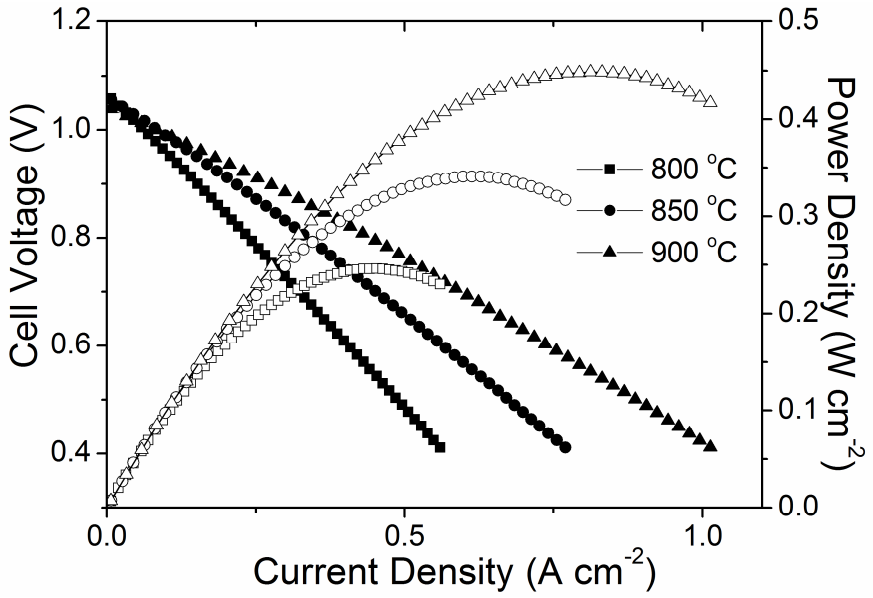

Figure S14. V-I curves of K-PSCF-CFA|YSZ|BCFN tested from 800 °C to 900 °C with 40 ml min^{-1} H_2 flow rate. The YSZ-electrolyte supported button cells with the cell configuration of K-PSCFN-CFA|ZSY|BCFN has been fabricated by brushing the P-PSCFN ink on one surface and the BCFN ink on the other surface of the YSZ electrolyte pellet (~ 300 μm thickness) and sintering the electrode in air at 900 ^oC for 2 h. P-PSCFN converted to K-PSCFN-CFA when the anode was exposed to H_2 at 900 ^oC for 1 h.

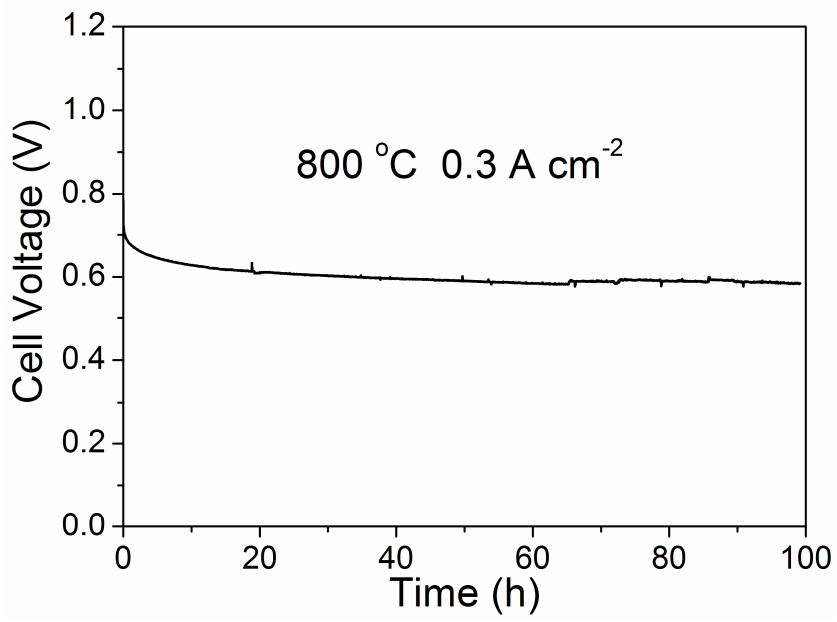

Figure S15. Cell voltage as a function of time of K-PSCFN-CFA|YSZ|BCFN tested at 800 °C under constant current of 0.3 A cm^{-2}.

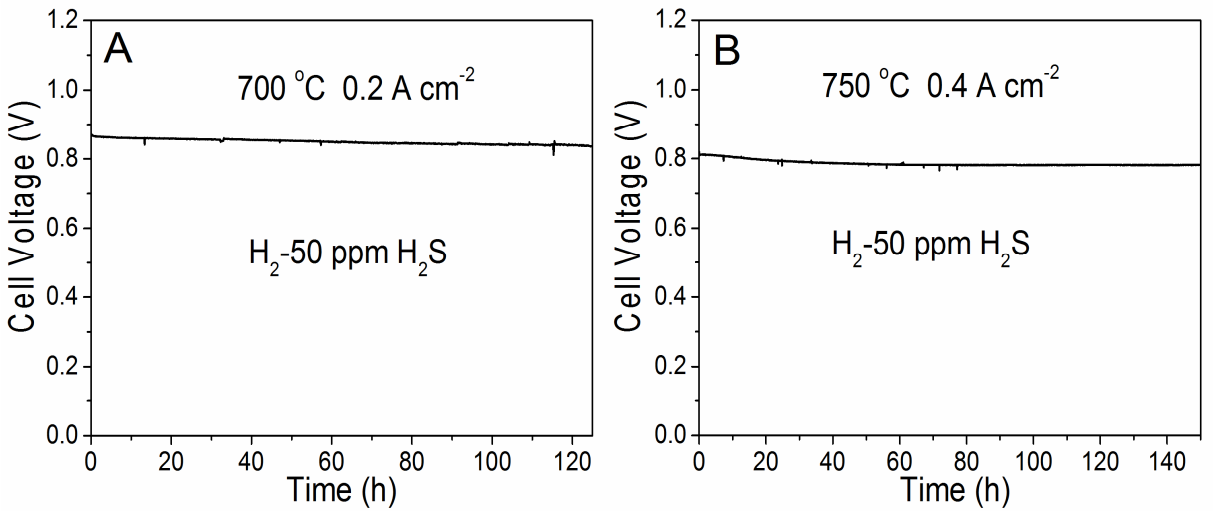

Figure S16. Cell voltage as a function of time for the K-PSCFN-CFA|LSGM|P-PSCFN cells operated under a constant current load of (**A**) 0.2 and (**B**) 0.4 A cm^{-2} in H_2-50 ppm H_2S at 700 and 750 °C, respectively.

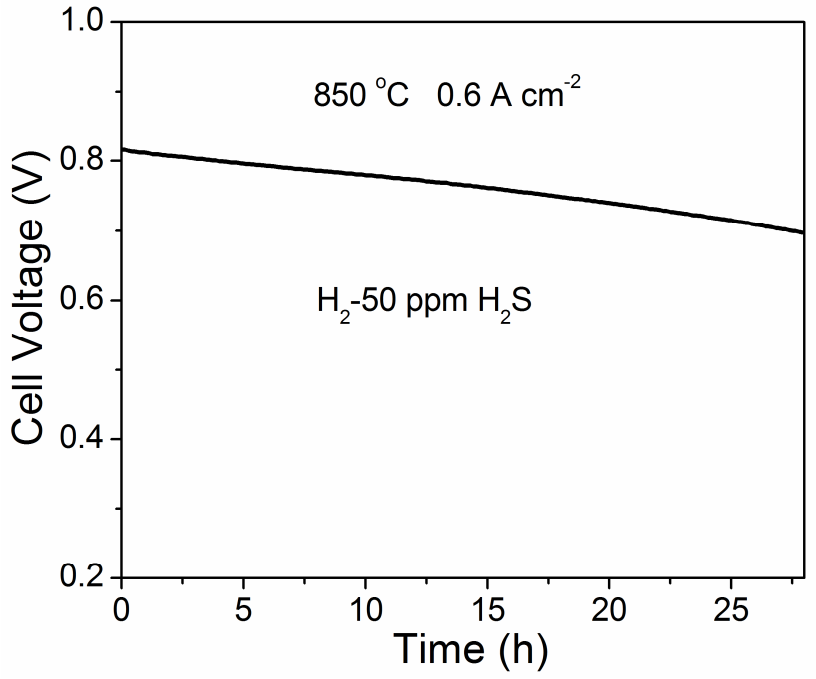

Figure S17. Cell voltage of single cells with the cell configuration of Ni-GDC|LSGM|BCFN operated under constant current load of 0.6 A cm^{-2} in H_2 containing 50 ppm H_2S at 850 ^oC.